# Cell shape and contractility regulate ciliogenesis in cell cycle–arrested cells

Amandine Pitaval,[1] Qingzong Tseng,[2] Michel Bornens,[3] and Manuel Théry[2]

[1]Laboratoire Biopuces, Institut de Recherche en Sciences et Technologies pour le Vivant, Direction des Sciences du Vivant, Commissariat à l'Energie Atomique et aux Energies Alternatives, 38054 Grenoble, Cedex 09, France
[2]Laboratoire de Physiologie Cellulaire et Végétale, Institut de Recherche en Sciences et Technologies pour le Vivant, Commissariat à l'Energie Atomique et aux Energies Alternatives, Centre National de la Recherche Scientifique, Université Joseph Fourier, Institut National de la Recherche Agronomique, 38054 Grenoble, Cedex 09, France
[3]Institut Curie, Unité Mixte de Recherche144, Centre National de la Recherche Scientifique, 75006 Paris, Cedex 05, France

In most lineages, cell cycle exit is correlated with the growth of a primary cilium. We analyzed cell cycle exit and ciliogenesis in human retinal cells and found that, contrary to the classical view, not all cells exiting the cell division cycle generate a primary cilium. Using adhesive micropatterns to control individual cell spreading, we demonstrate that cell spatial confinement is a major regulator of ciliogenesis. When spatially confined, cells assemble a contractile actin network along their ventral surface and a protrusive network along their dorsal surface. The nucleus–centrosome axis in confined cells is oriented toward the dorsal surface where the primary cilium is formed. In contrast, highly spread cells assemble mostly contractile actin bundles. The nucleus–centrosome axis of spread cells is oriented toward the ventral surface, where contractility prevented primary cilium growth. These results indicate that cell geometrical confinement affects cell polarity via the modulation of actin network architecture and thereby regulates basal body positioning and primary cilium growth.

## Introduction

Tissue development and renewal rely on the spatial and temporal regulation of the balance between cell growth and quiescence. Most cells in tissues are quiescent. In vertebrates, these cells generally possess a primary cilium (Gerdes et al., 2009). It is widely considered that ciliogenesis is tightly coupled to the cell cycle (Wheatley, 1971; Santos and Reiter, 2008). In postmitotic cells entering the G0 phase, the mother centriole differentiates into a basal body, anchoring itself to the plasma membrane and growing the cilium (Alieva and Vorobjev, 2004). When quiescent cells resume cell cycle, the cilium is resorbed (Tucker et al., 1979; Pugacheva et al., 2007). According to this classical view, quiescent cells are ciliated, whereas nonciliated cells are engaged in the cell cycle. However, several examples of differentiated, but not ciliated, cells in situ suggest that cell cycle exit might not be sufficient to induce ciliogenesis (Seeley and Nachury, 2010). The parameters regulating ciliogenesis in growth-arrested cells remain to be elucidated.

It has been concluded from experiments on cultured cells that cell cycle arrest and cell confluence are required for ciliogenesis (Wheatley et al., 1994). Primary cells progressively stop cycling after a limited number of passages, and immortalized cell lines stop cycling upon serum starvation and deprivation of growth factors. In both cases, a high level of confluence seems necessary to grow the primary cilium (Alieva and Vorobjev, 2004). However, because contact inhibition in confluent cells is known to induce cell growth arrest, it is not clear whether confluence affects ciliogenesis by promoting cell quiescence or by playing a more direct role on ciliogenesis. We designed specific tools and methodology to control separately the degree of cell confluence and cell cycle exit. We then analyzed the parameters governing ciliogenesis in cell cycle–arrested cells.

## Results and discussion

Human retinal pigment epithelial (RPE1) cells are diploid immortalized cells that maintain normal checkpoints on cell cycle progression as well as contact inhibition of growth. We confirmed the role of cell confluence in ciliogenesis in these cells

Correspondence to Manuel Théry: manuel.thery@cea.fr

Abbreviation used in this paper: RPE1, human retinal pigment epithelial.



The Rockefeller University Press $30.00
J. Cell Biol. Vol. 191 No. 2 303–312
www.jcb.org/cgi/doi/10.1083/jcb.201004003

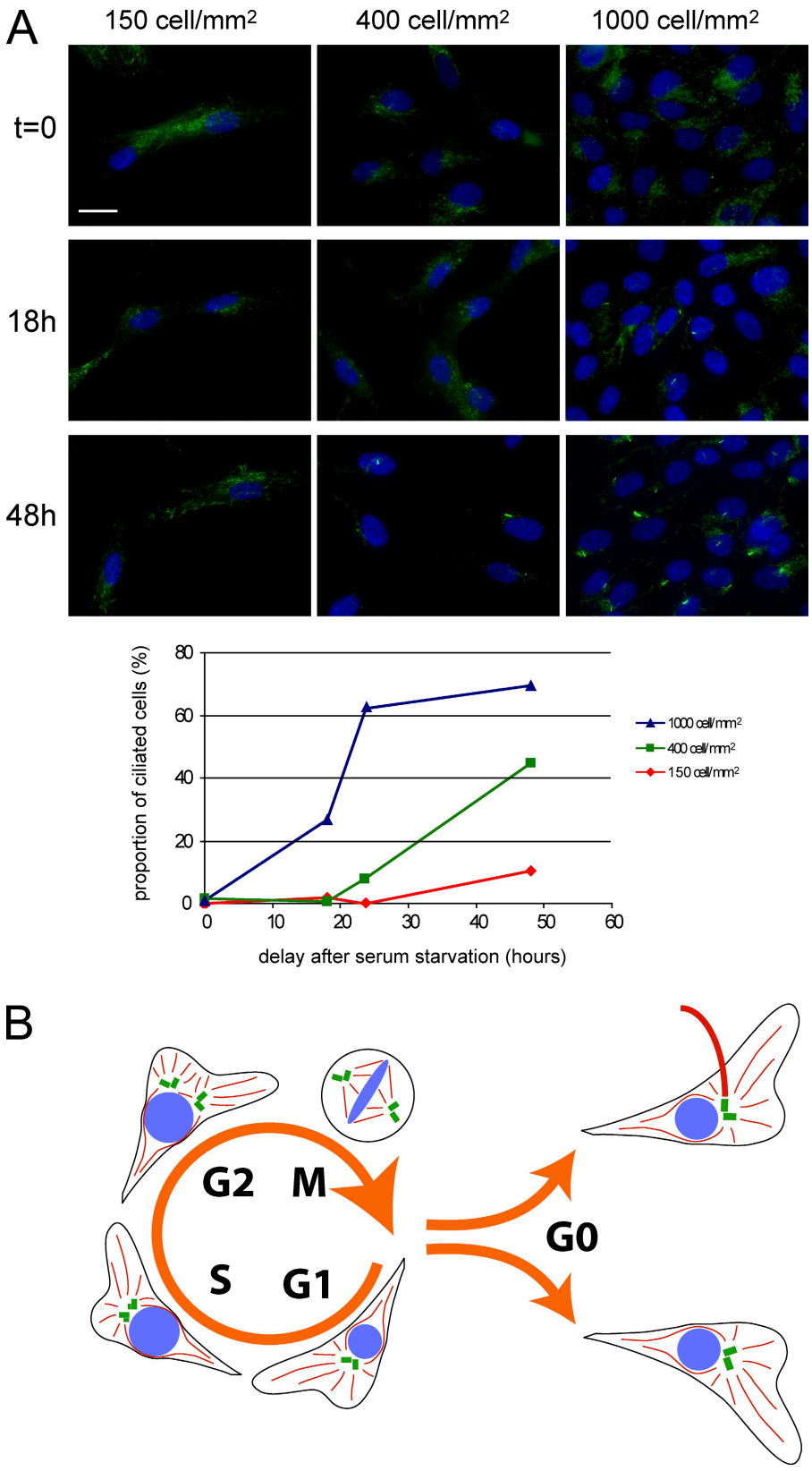


Figure 1. **Growth arrest, confluency, and ciliogenesis.** (A) RPE1 cells were plated on polystyrene-coated glass coverslips at various densities and serum starved. At different time points, cells were fixed and labeled for acetylated tubulin (green) to reveal primary cilia and DNA (blue). The graph shows the quantification of the proportion of ciliated cells in these conditions (the number of quantified cells is given for every time point: 150 cells/mm$^2$, $n$ = 20, 50, 58, and 34; 400 cells/mm$^2$, $n$ = 118, 183, 101, and 171; and 1,000 cells/mm$^2$, $n$ = 174, 312, 108, and 166). Bar, 10 µm. (B) Working model: cells can adopt two distinct states in G0 with or without growing a primary cilium.

by plating RPE1 cells at various densities. Coverslips were then fixed at various time points after serum starvation and stained for primary cilium (Alieva et al., 1999). Few cells had primary cilium soon after starvation. However, 48 h later, a majority of confluent cells had a cilium, whereas only a small proportion of dispersed cells had one (Fig. 1 A). We checked by video microscopy during 48 h that most cells had actually stopped dividing at all densities. This demonstrated that cells could exit the cycle

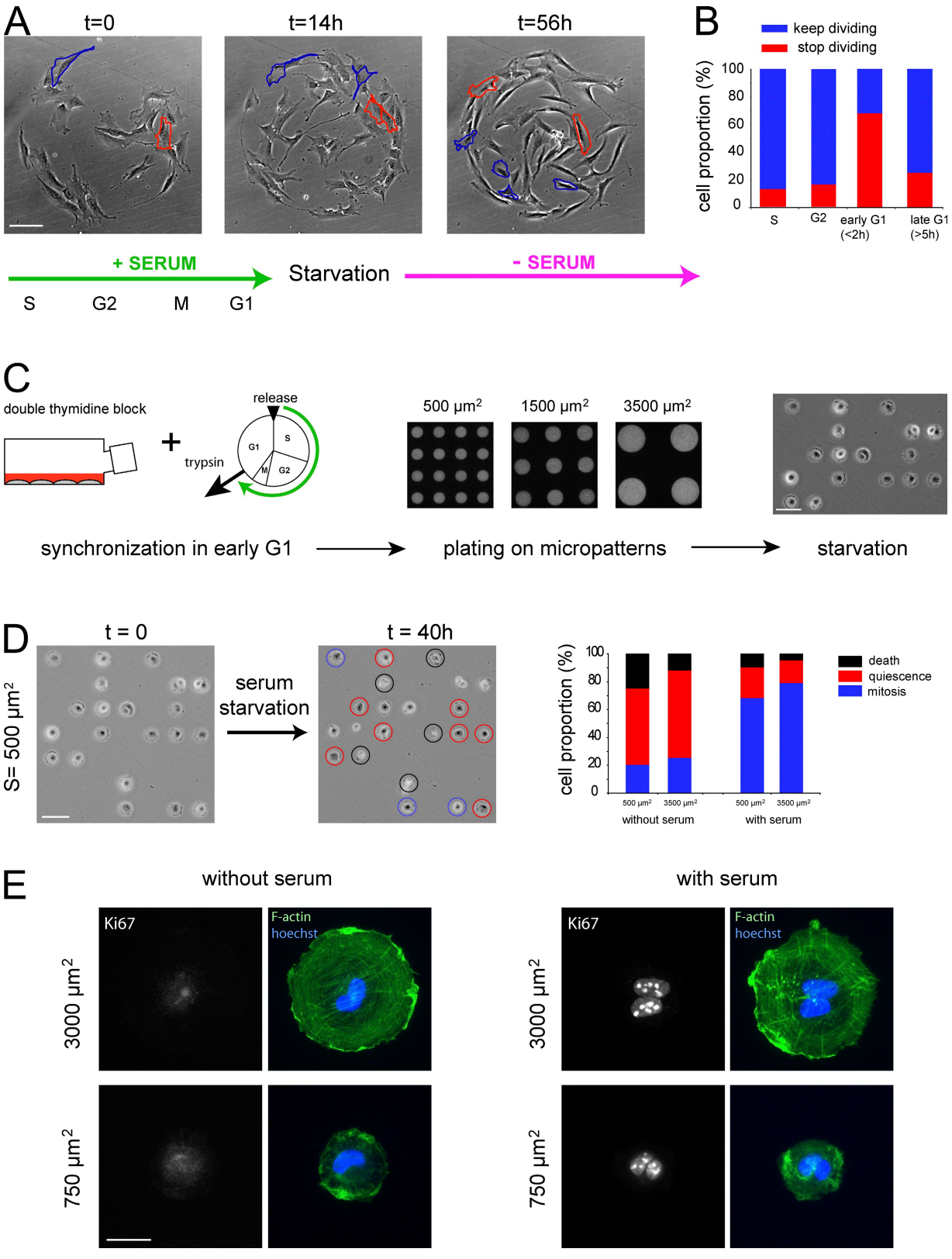


Figure 2. **Cell cycle exit in G1.** (A) Cells were plated on large, fibronectin-coated discoidal micropatterns to prevent them from escaping the observation field. They were monitored by time-lapse microscopy to measure cell division time with respect to the time of starvation and to follow the fate of daughter cells. The red cell illustrates starvation in early G1: the cell divided 2.5 h before starvation and stopped dividing after. The blue cell illustrates starvation in late G1: the cell divided 5 h before starvation and divided again after. See corresponding Video 1 and Fig. S1. Bar, 100 µm. (B) The histogram shows the proportion of dividing and nondividing cells, depending on the cell cycle stage when starvation occurred (S, $n = 31$; G2, $n = 31$; early G1 [<2 h after mitosis], $n = 92$; and late G1 [>5 h after mitosis], $n = 130$). (C) Experimental procedure used for the following experiments. Cells were synchronized in early G1, plated on a micropatterned coverslip with 10 different sizes of discs ranging from 500 to 3,500 µm², and serum starved. Bar, 50 µm.

with or without growing a primary cilium (Fig. 1 B) and that specific parameters associated with cell confluence seemed to regulate this fate.

We further investigated the role of cell spatial confinement and the presence of cell–cell contact on ciliogenesis by plating individual cells on micropatterned surfaces of defined sizes. To analyze cell cycle exit and ciliogenesis in these conditions, it was necessary to determine the exact time window in which cells could be plated on micropatterns and serum starved to obtain cell cycle exit before any further division. Therefore, we investigated the cell response to serum starvation all along the cell division cycle (Fig. 2 A and Fig. S1). As expected from previous studies (Pardee, 1974; Zetterberg and Larsson, 1985), most cells starved in early G1 did not reenter the cell cycle (Fig. 2 B). We thus proceeded as follows: cells were synchronized in early G1, plated on individual micropatterns, and starved. The role of cell confinement was tested by using an array of discoidal micropatterns of various sizes ranging from 500 to 3,500 $\mu m^2$ (Fig. 2 C).

Because cell spreading has been shown to positively regulate cell cycle progression (Chen et al., 1997; Huang et al., 1998; Schwartz and Assoian, 2001), we checked whether RPE1 cells actually left the cell cycle on all micropattern sizes. Just after spreading, cells were starved and monitored by video microscopy. Cells on small or large micropatterns left the cell cycle in similar proportions (Fig. 2, D and E). Control nonstarved cells kept on dividing. We concluded that cell cycle exit was specifically induced by serum starvation independently of the extent of cell spreading.

Dramatic differences in the ciliation rate 48 h after serum starvation were observed, depending on the size of the micropatterns. Although cilia were present on most cells confined on small micropatterns, they became less frequent as cell spreading increased (Fig. 3, A and B). Most of the highly spread cells had exited cell cycle without growing a cilium. Instead, these cells displayed a large network of acetylated microtubules in their cytoplasm. In addition, the mean primary cilium length decreased from 5 to 2 µm as cell spreading increased (Fig. 3 C). Long cilium, >6 µm, could only be observed in spatially confined cells. These differences were already present 24 h after starvation and maintained for at least 72 h (Fig. 3, D and E), suggesting they were not caused by a delay in basal body maturation (Anderson and Stearns, 2009). When two cells were found on the same micropattern, each cell adopted half of the area, and their ciliation rate matched that of individual cells on micropatterns twice as small (Fig. 3 B). Therefore, cell–cell contact did not seem to be required for, nor regulate, ciliogenesis in these cells. Until now, primary cilium growth defects in cell cycle–arrested cells had only been seen in cells in which basal body integrity (Graser et al., 2007; Mikule et al., 2007), centrosome-associated cell cycle regulation (Spektor et al., 2007), or intraflagellar transport (Schneider et al., 2005) required for ciliogenesis was specifically impaired. Our results demonstrate a strong dependency of ciliogenesis on the degree of cell shape extension in wild-type cells.

The degree of cell spreading affects actin network architecture. As cell spreading increased, cells displayed larger transversal stress fibers and more circumferential bundles (Fig. 3 A). Because actin dynamics have been shown to affect ciliogenesis (Kim et al., 2010), we tested whether these actin structures were involved in the cell shape–associated regulation of primary cilium growth by disrupting actin network integrity with 1 µM cytochalasin D. Several large cells managed to maintain their spreading, whereas their actin network was damaged. Interestingly, after a 24-h starvation in the presence of cytochalasin D, most cells, regardless of their size, were ciliated (Fig. 4 A). In addition, cilium length was no longer reduced in large cells; instead, large cells had slightly longer cilia. The actin network, therefore, appeared fully responsible for the regulation of ciliogenesis in response to cell shape extension.

We then looked for more specific actin structures that could be implicated in this regulation. The location of myosin II strongly affects actin network architecture and thus plays a key role in the establishment of cell polarity at all stages of organism development (St Johnston and Ahringer, 2010). In epithelial cells, ezrin is restricted to the apical pole where, upon phosphorylation, it links the polymerizing actin meshwork in membrane protrusion to the plasma membrane (Dard et al., 2004; Fievet et al., 2004). After 24 h of serum starvation, RPE1 cells confined on small micropatterns displayed a polarized actin network with myosin II–positive actin bundles at their ventral surface and an ezrin-rich actin meshwork at their dorsal surface (Fig. 4 B and Fig. S2). In extended cells, the actin network architecture appeared less polarized. Ezrin staining at the cell dorsal surface appeared fainter and more dispersed. Most actin structures were strongly decorated with myosin II (Fig. 4 B and Fig. S2). Indeed, cell shape extension has been correlated to high levels of actomyosin contraction (McBeath et al., 2004; Polte et al., 2004). Because up-regulation of RhoA in response to the loss of meckelin, a transmembrane protein of the primary cilium, has been shown to induce the formation of stress fibers and prevent primary cilium growth (Dawe et al., 2009), high levels of contraction could be responsible for the impaired ciliogenesis in spread cells.

To test this hypothesis, cell contractility was inhibited with either 10 µM Y27632, to inactivate Rho kinase, or with 50 µM blebbistatin, to inactivate myosin II ATPase. Both treatments induced actomyosin relaxation of spread cells as revealed by the large reduction of phosphomyosin II staining (Fig. 4 B). Interestingly, the proportion of ciliated cells in relaxed spread cells

(D) G1-starved cells on micropatterns were observed in time-lapse phase-contrast microscopy over 40 h. The proportion of dividing cells (blue), nondividing cells (red), and dying cells (black) were quantified in cells plated on the smallest (500 $\mu m^2$) and largest (3,500 $\mu m^2$) micropatterns in the presence ($n$ = 116 and 43, respectively) or absence ($n$ = 123 and 115, respectively) of serum. No clear difference could be observed between the two cell sizes. Bar, 50 µm. (E) Cell quiescence. Cells were plated on micropatterns with or without serum, fixed, and stained for Ki67 (proliferation marker), F-actin (green), and DNA (blue). A large majority of individual cells on small and large micropatterns were quiescent after 24 h of serum starvation, as revealed by their negative Ki67 staining (75%, $n$ = 102; and 79%, $n$ = 174; respectively). Cells proliferated in the presence of serum and were mostly Ki67 positive. Bar, 10 µm.

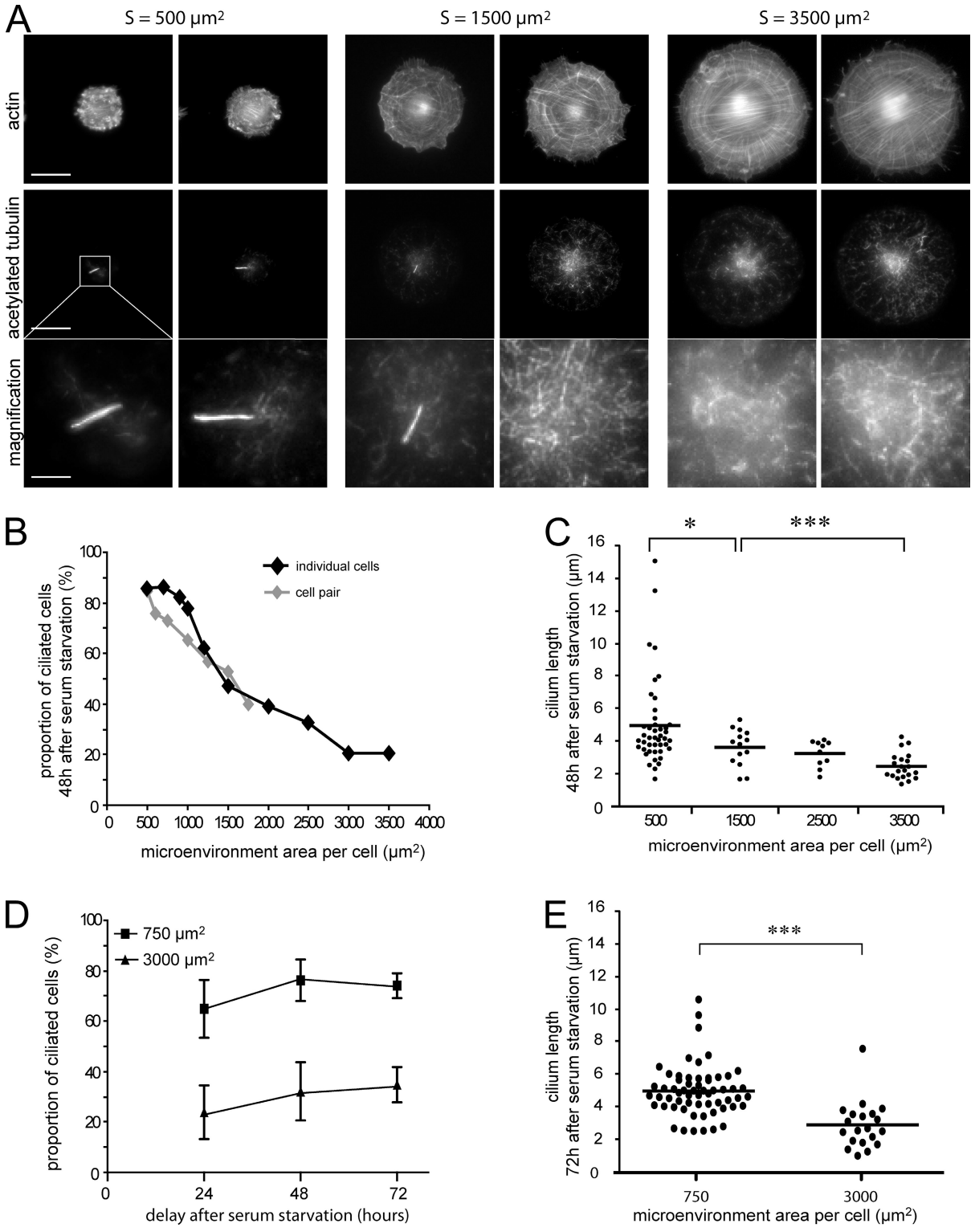


Figure 3. **Cell confinement and ciliogenesis.** The experimental procedure for all panels is described in Fig. 2 C. (A) Cells on various micropattern sizes were serum starved for 48 h, fixed, and stained for F-actin (top) and acetylated tubulin (bottom with an inset magnification) to reveal the primary cilium. Two examples of cells on 500, 1,500, and 3,500 µm² are shown to illustrate that most cells on 500 µm² had a primary cilium, half had one on 1,500 µm², and most cells on 3, 500 µm² had no primary cilium. Bars, 20 µm. Inset bar, 4 µm. (B) The proportion of individual ciliated cells on 10 different micropattern sizes ($n > 100$ for each) is shown with the black curve. The proportion of ciliated cells in cell doublets (two cells per pattern) on 10 different micropattern sizes ($n > 100$ for each) is shown with the gray curve with respect to individual cell size. (C) Quantification of primary cilium length depending on micropattern size. Primary cilium length was shorter in larger micropatterned cells. (D) Quantification of ciliated cell frequency in cells plated on small (750 µm²) and large (3,000 µm²) micropatterns over time ($n > 170$ for each). The rate slightly increased from 24 to 48 h and then reached a plateau. (E) Quantification of primary cilium length on small (750 µm²) and large (3,000 µm²) micropatterns 72 h after serum starvation. Primary cilium length was similar to the one measured 24 h after serum starvation (compare with C). *, $P < 0.05$ and ***, $P < 0.001$. Plotted bars represent standard deviations. Horizontal bars represent mean values.

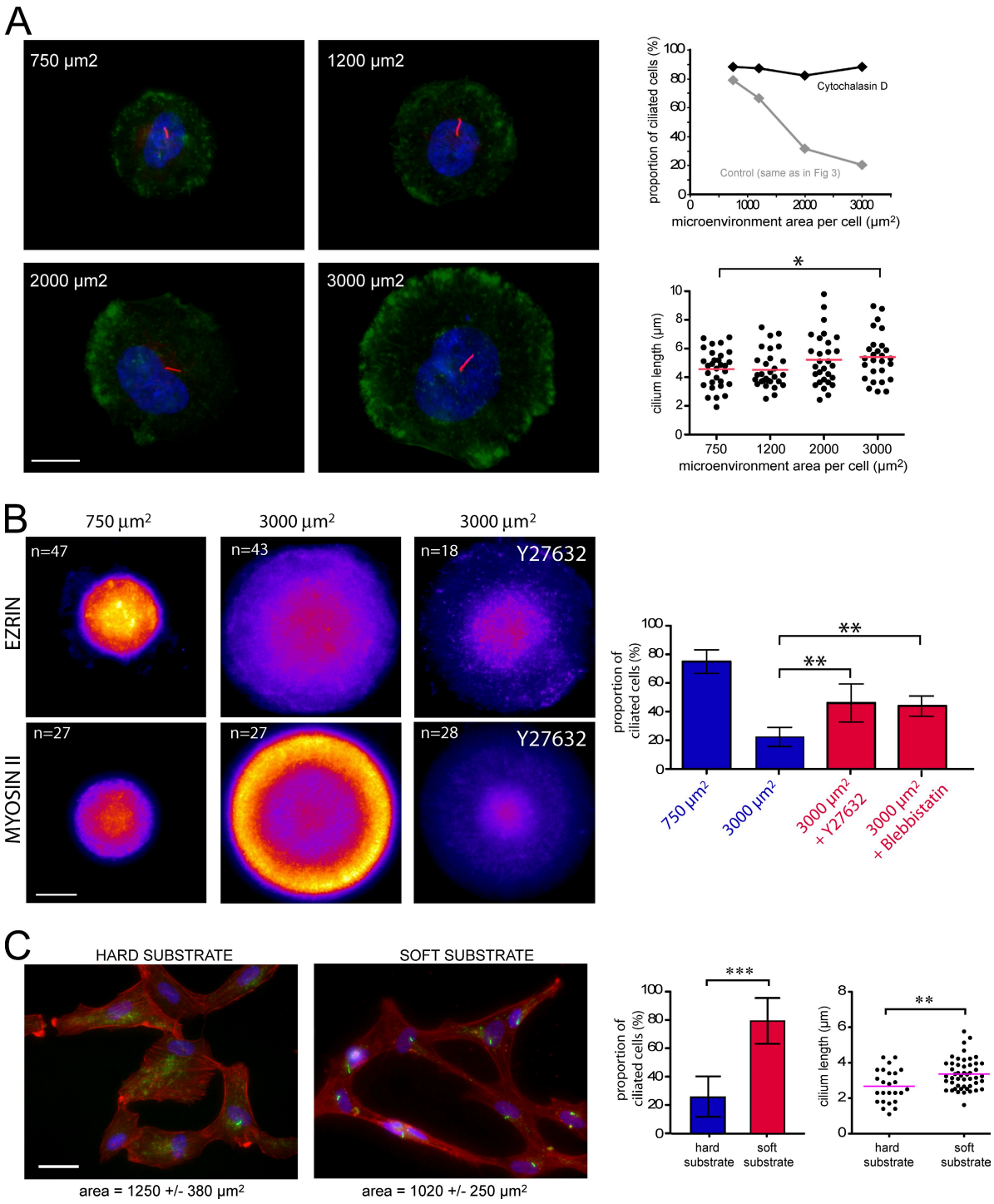


Figure 4. **Actin network assembly, contractility, and ciliogenesis.** The experimental procedure for A and B is described in Fig. 2 C. RPE1 cells were plated on micropatterns (from 750 to 3,000 µm²) and serum starved for 24 h. (A) Micropatterned cells were treated with cytochalasin D during starvation. Cells were fixed and stained for acetylated tubulin (red), F-actin (green), and DNA (blue). Primary cilium occurrence (top, *n* = 82, 97, 82, and 41) and length (bottom, *n* = 30, 26, 27, and 25) were measured in cells whose shape still covered the entire micropattern after the treatment. Bar, 5 µm. (B) Micropatterned cells were treated with either Y27632 or blebbistatin during starvation. Cells were then fixed and immunolabeled for phosphoezrin (top) and phosphomyosin II (bottom). Z acquisitions were performed and projected on a single image containing the maximal intensity of each pixel. Several images on each micropattern were averaged and color coded with the fire look-up table to highlight intensity variations. Bar, 5 µm. Primary cilium occurrence was measured in each condition (*n* > 400 for each). (C) RPE1 cells in early G1 were plated at low density on hard substrate (polystyrene-coated glass coverslips) or soft substrate (polyacrylamide gel grafted on glass coverslips). Cells were then serum starved for 48 h, fixed, and stained for F-actin (red), DNA (blue), and acetylated tubulin (green). Most cells on hard substrates had no primary cilium (left). A majority of cells on soft substrates were ciliated (right). Primary cilium occurrence was measured at a cell density of 200 cells/mm² on hard substrates (*n* = 300) and on soft substrates (*n* = 1,140). Primary cilium length was shorter on hard substrates than on soft ones. *, P < 0.05; **, P < 0.01; and ***, P < 0.001. Plotted bars represent standard deviations. Horizontal bars represent mean values. Bar, 20 µm.

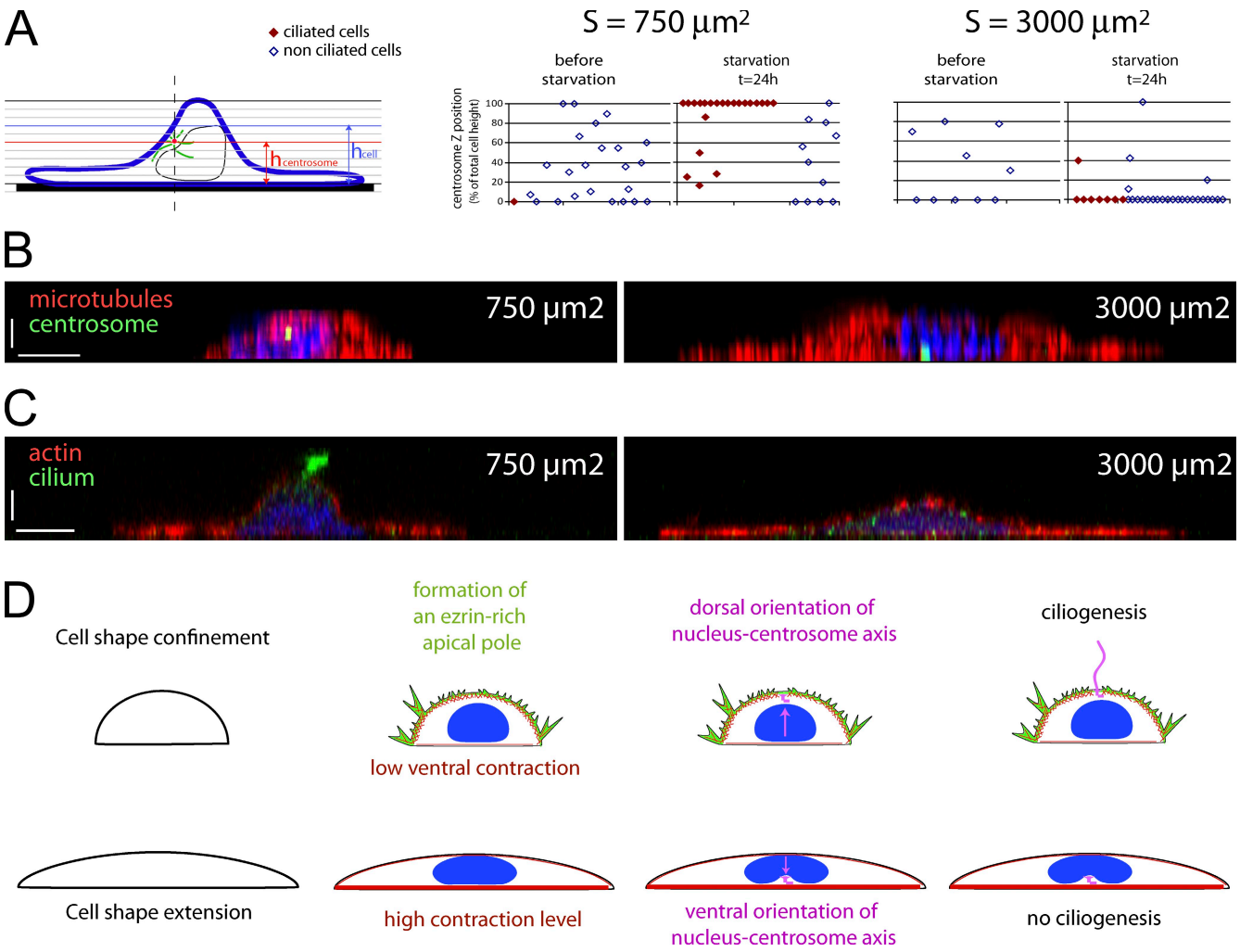


Figure 5. **Cell shape regulates cell polarity and ciliogenesis.** The experimental procedure is described in Fig. 2 C. RPE1 cells were plated on small (750 µm$^2$) and large (3,000 µm$^2$) micropatterns and serum starved for 24 h. (A) Micropatterned cells were fixed and immunolabeled to reveal primary cilium, centrosome/basal body, actin filaments, and nucleus (Fig. S3 A). Z stacks were performed to measure centrosome position. The ratio between centrosome position and local cell height was measured in confined and extended cells before and 24 h after serum starvation in ciliated and nonciliated cells. (B) Micropatterned cells were fixed in cold methanol and immunolabeled for γ-tubulin to reveal the centrosome (green) and immunolabeled with α-tubulin to reveal microtubules (red). DNA is in blue. Z stacks were acquired and deconvolved to detect centrosome positioning (Fig. S3 B). XZ optical sections illustrate centrosome positioning above the nucleus in confined cells (left) and below the nucleus in spread cells (right). (C) Micropatterned cells were fixed with paraformaldehyde, immunolabeled for acetylated tubulin (green), and stained with phalloidin (red; Fig. S3 C). DNA is in blue. XZ optical sections illustrate the presence of the primary cilium at the dorsal surface of confined cells (left) and the presence of acetylated microtubules in the cytoplasm of spread cells (right). (D) Results summary. When cells are spatially confined, they develop a polarized actin architecture with contractile bundles in the ventral surface and a polymerizing network in membrane protrusions at the dorsal surface. In these cells, the nucleus–centrosome axis is reproducibly oriented toward the dorsal surface in a Rho kinase–dependent manner. The apical positioning of the centrosome and its anchoring in the ezrin-rich actin network promote the formation of the primary cilium. When cells are highly extended, the actin network is unbalanced toward the formation of numerous and large contractile bundles. The internal polarity is reversed compared with confined cells. The nucleus–centrosome axis is oriented toward the ventral surface in an actin- and microtubule-dependent manner. The centrosome is in close proximity to actin stress fibers, whose contractility prevents the extension of the primary cilium. X bars, 5 µm. Z bars, 2 µm.

was twice that of control spread cells in both cases (Fig. 4 B). It is noteworthy that no significant effect could be detected on mean primary cilium length (control: 2.9 ± 1.5 µm, $n = 20$; blebbistatin: 2.9 ± 1 µm, $n = 30$; and Y27632: 3.6 ± 1 µm, $n = 30$).

To further confirm the negative regulation of cell contraction on ciliogenesis, we plated cells on soft substrates to release cell contraction (Polte et al., 2004; Engler et al., 2006; Solon et al., 2007). Cells displayed large and straight stress fibers on hard substrates but thinner and looser bundles on soft substrates (Fig. S2 D). Strikingly, although only 25% of sparsely populated cells had a primary cilium on hard substrate (polystyrene), almost 80% were ciliated on soft substrates (polyacrylamide gel; Fig. 4 C). In addition, cilia were longer. Altogether, these results demonstrated that, in quiescent cells, the high level of contraction associated with cell spreading hindered ciliogenesis.

Rho kinase is also known to regulate centrosome positioning (Chevrier et al., 2002). Because early stages of ciliogenesis rely on basal body migration and docking to the plasma membrane, we wondered whether actin architecture and myosin II activity could play a role in basal body positioning. After serum starvation, the basal body was found to migrate above

the nucleus, to the ezrin-rich cell dorsal surface of confined cells, where they could grow a primary cilium. However, in starved spread cells, basal bodies were found below the nucleus, in contact with the ventral surface where they rarely formed a primary cilium (Fig. 5, A–C and Fig. S3 B). Dorsal positioning of basal body and ciliogenesis appeared to be tightly coupled (Fig. S3 D). After cytochalasin D treatment, basal bodies adopted a dorsal position, and ciliogenesis was improved (Fig. S3, B and D). After Rho kinase inhibition in confined cells, basal bodies were positioned below the nucleus, and ciliogenesis was reduced (Fig. S3, B and D). Inhibition of cell contractility in confined cells did not affect cilium length (control: 5 ± 1.5 µm, $n = 60$; Y27632: 5.3 ± 2 µm, $n = 37$; and blebbistatin: 5.1 ± 2.5 µm, $n = 34$). As previously suggested from RhoA inhibition in multiciliated cells (Park et al., 2006; Pan et al., 2007), this showed that Rho kinase activity is necessary for the apical positioning of the basal body and the subsequent growth of the primary cilium. However, in extended cells, Rho kinase inhibition did not affect the ventral positioning of basal bodies but promoted the growth of ventral cilia. This showed that cell contractility acts separately on both cilium extension and basal body positioning.

In this study, we thus report a major role for physical parameters such as spatial confinement and substrate rigidity, which, through their effect on actin cytoskeleton architecture, regulate ciliogenesis at cell cycle exit (Fig. 5 D). When individual cells were sufficiently spatially confined on adhesive substrate, they could assemble both a contractile ventral domain and a protrusive, ezrin-rich dorsal domain mimicking the apicobasal polarity of epithelial cells. This polarization was further transmitted to the internal cell organization with the nucleus–centrosome axis oriented toward the dorsal surface in a Rho kinase–dependent manner. Under these conditions, most cells assemble a primary cilium. When individual cells were highly spread, they mostly formed a highly contracted actin network in contact with their adhesive substrate. In this case, the internal polarity was reversed: the nucleus–centrosome axis was oriented toward the ventral surface. In this position, below the nucleus, and in proximity with stress fibers, the centrosome could not induce the growth of the primary cilium. This was partially a result of the local contractility of the cell cortex. Overall, these results demonstrate that cell cycle exit is not sufficient to induce primary cilium growth. Depending on the global organization of actin cytoskeleton architecture and dynamics, cells can enter a quiescent state with or without assembling a primary cilium. Whether such a regulation occurs during development could have far-reaching consequences given the sensory functions of primary cilia.

## Materials and methods

### Cell culture

Human telomerase-immortalized, retinal-pigmented epithelial cells (hTERT-RPE1; Takara Bio Inc.) were grown at 37°C and 5% $CO_2$ in DME/F12 (Invitrogen) containing 10% fetal calf serum, 2 mM glutamine, 100 U/ml penicillin, and 100 U/ml streptomycin. We used a double thymidine block to synchronize cells at the G1/S transition. Cells in a culture flask were treated with 5 mM thymidine for 16 h, released for 8 h with normal culture medium, and then were treated again with thymidine for 16 h.

To detect cilium incidence of G1-enriched cells on micropatterns, cells were trypsinized just after mitosis (10 h after release of G1/S synchronization) and plated on the micropatterned coverslip (10,000 cells/cm$^2$) to obtain a majority of patterns with individual cells. Medium was gently flushed over cells and replaced with fresh medium 0.5–1 h later to remove nonattached cells in suspension. Serum was then removed 1 h later, and cells were cultured for 24–72 h.

Cytoskeletal drugs were added to the medium when the serum was removed, i.e., 2 h after the plating of cells on micropatterns. For Rho kinase inhibition, Y27632 was added at 10 µM. For myosin II ATPase inhibition, blebbistatin was added at 50 µM. For actin network destabilization, cytochalasin D was added at 1 µM 2 h after serum removal to allow starved cells to fully spread on large micropatterns before being treated.

### Micropatterning

Glass coverslips were first spin coated with an adhesion promoter (TI Prime; MicroChemicals) and then with 0.5% polystyrene dissolved in toluene at 3,000 rpm for 30 s. The polystyrene layer was further oxidized with an oxygen plasma treatment (FEMTO; Diener Electronics) for 10 s at 30 W and incubated with 0.1 mg/ml polylysine poly-ethylene-glycol (JenKem Technology) in 10 mM Hepes, pH 7.4, at room temperature for 1 h. Coverslips were then dried by spontaneous dewetting. Poly-ethylene-glycol–coated slides were placed in contact with an optical mask containing the transparent micropatterns (Toppan Photomasks, Inc.) using a home-made vacuum chamber and exposed for 3 min to deep UV light (UVO Cleaner; Jelight Company). Micropatterned slides were washed once in PBS and finally incubated for 30 min with a solution of 20 µg/ml bovine fibronectin solution (Sigma-Aldrich) and 5 µg/ml Alexa Fluor 646– or Alexa Fluor 542–labeled fibrinogen (Invitrogen). Before plating cells, patterned coverslips were washed three times with sterilized PBS. We also used commercially available micropatterned glass coverslips (CYTOOChips; Cytoo).

### Soft substrate fabrication

Acrylamide monomer solution (Sigma-Aldrich) containing 5% acrylamide and 0.13% bisacrylamide was polymerized by ammonium persulfate (Sigma-Aldrich) and *N,N,N,N*-tetramethylethylenediamine (Sigma-Aldrich) over a glass coverslip previously silanized with 3-(trimethoxysilyl)propyl methacrylate (Sigma-Aldrich). 25 mM 4-benzoylbenzyl-trimethylammonium chloride (benzophenone; custom synthesis by Sigma-Aldrich outsourced to Labotest) and fibronectin at 40 µg/ml in PBS were added on the surface of the polymerized gel and then exposed to UV light (Delolux 03 S; Supratec) at 400 W for 45 s to graft the fibronectin using the photoactivation of benzophenone (Fink et al., 2007). The gel was washed with PBS before cell seeding.

### Video microscopy and cell imaging

Time-lapse acquisitions were taken with an inverted microscope (Axiovert 200M; Carl Zeiss, Inc.). The temperature, $CO_2$, and humidity control were performed using a Box and Brick system (Life Imaging Services). Multiple positions were recorded using an XY motorized stage (Marzhauser) with a 10-min time frame over 40–54 h with a dry 10× phase-contrast objective. Fluorescence images were taken using an upright microscope (BX61; Olympus). Cilium frequency was manually calculated on images taken either with a dry 20× objective (NA = 0.4) or with a dry 40× objective (NA = 0.9). Fluorescent images shown are maximal projections of Z stacks acquired with oil immersion objectives at either 63× or 100× (NA = 1.4) mounted on a piezo ceramic (Physics Instruments). Both microscopes were controlled with Metamorph software (MDS Analytical Technologies). Side views were obtained using XZ optical sections (not projections) of either classical epifluorescence Z stacks with a piezo or confocal Z stacks (15 planes separated by 500 nm) acquired with a confocal microscope (TCS-SP2; Leica) through a 63× objective (NA = 1.4).

### Immunostaining

For immunostaining experiments, cells were plated on polystyrene-coated glass coverslips to promote cell attachment and keep a good optical quality. Coating was performed by spin coating 0.5% polystyrene solution in toluene at 3,000 rpm for 30 s. The polystyrene layer was further oxidized with an oxygen plasma treatment. Alternatively, cells were plated on micropatterned or soft substrates.

For actin-associated protein and primary cilium immunostaining, RPE1 cells were fixed in 4% paraformaldehyde in cytoskeleton buffer, pH 6.1, for 15 min at room temperature without any prior PBS wash. They were then rinsed twice with PBS and incubated in 0.1 M ammonium chloride in PBS for 10 min. Cells were then permeabilized in 0.1% Triton X-100 in PBS

for 3 min and blocked with 3% BSA in PBS for 30 min. For phosphomyosin immunostaining, cells were prepermeabilized for 15 s with 0.1% Triton X-100 in cytoskeleton buffer before paraformaldehyde fixation. For centrosome detection, cells were fixed for 5 min in methanol at −20°C. For Ki67 immunostaining, cells were fixed with 4% paraformaldehyde in PBS, pH 7.4, for 15 min at room temperature.

Primary monoclonal mouse antibodies against acetylated tubulin (1:10,000 dilution; Sigma-Aldrich) and α-tubulin (1:1,000; AbD Serotec) and primary polyclonal rabbit antibodies against phosphomyosin light chain 2 (1:100; Cell Signaling Technology), γ-tubulin (1:500; Abcam), and Ki67 (1:50; Invitrogen) were added in blocking buffer (1.5% BSA) for 1 h at room temperature. Primary polyclonal rabbit antibodies against phosphoezrin (1:600; Cell Signaling Technology) were added in blocking buffer overnight at 4°C.

The secondary antibodies Cy3- and Cy5-conjugated goat anti–mouse, goat anti–rat, and goat anti–rabbit (AffiniPure; Jackson ImmunoResearch Laboratories, Inc.) were used at a dilution of 1:500 in 1.5% BSA and incubated with 1 µg/ml FITC-conjugated phalloidin (Sigma-Aldrich) for 45 min in the dark at room temperature. Cells were incubated in 0.2 µg/ml Hoechst for 5 min in PBS before mounting in Mowiol (Sigma-Aldrich).

### Image processing

All of the images were processed using ImageJ (National Institutes of Health). For 3D reconstruction, images were first deconvolved using the 3D iterative deconvolution plugin by theoretical point-spread function. For the cilium images at low magnification (Fig. 1), maximum projection of Z stacks or the plugin Extended Depth of Focus was applied to visualize all the cilium in a single plane.

### Quantification on images and statistical analysis

Fluorescence densities were measured on individual cells. Z stacks containing 20 images separated by 500 nm were projected along the Z axis using the maximal intensity of each pixel. We then quantified the ratio between the total fluorescence intensity and the cell area. The mean value of the image background around the cell was then subtracted from this value.

Compared experiments were performed together: cells were issued from a single pool and further fixed and immunolabeled with the same solution. Similarly, compared images were acquired the same day with the same acquisition parameters. Comparison between two sets of measures was performed using Student's *t* test (two tailed, 95% interval confidence: *, $P < 0.05$; **, $P < 0.01$; ***, $P < 0.001$). Plotted bars represent standard deviations. *n* refers to the total number of measures.

### Online supplemental material

Fig. S1 shows the analysis of cell cycle exit. Fig. S2 shows the quantification of ezrin and myosin II densities in confined and extended cells. Fig. S3 shows the labeling and quantification of centrosome position. Video 1 shows the monitoring of cell fate upon serum starvation. Online supplemental material is available at http://www.jcb.org/cgi/content/full/jcb.201004003/DC1.

We would like to thank Annie Delouvée for providing advice about RPE1 culture conditions, Véronique Collin-Faure for FACS analyses, Emilie Mercey for designing the optical mask, as well as Joanne Young, Laurent Blanchoin, Enrique De La Cruz, Denys Wheatley, Erica Golemis, Maxence Nachury, and Matthieu Piel for critical reading of the manuscript and discussions.

This work has been conducted thanks to the grant Agence Nationale pour la Recherche Jeune Chercheur attributed to M. Théry (ANR-08-JC-0103). The authors declare some conflict of interest because they are implicated in the company Cytoo, which commercializes micropatterns.

Submitted: 1 April 2010
Accepted: 13 September 2010

## References

Alieva, I.B., and I.A. Vorobjev. 2004. Vertebrate primary cilia: a sensory part of centrosomal complex in tissue cells, but a "sleeping beauty" in cultured cells? *Cell Biol. Int.* 28:139–150. doi:10.1016/j.cellbi.2003.11.013

Alieva, I.B., L.A. Gorgidze, Y.A. Komarova, O.A. Chernobelskaya, and I.A. Vorobjev. 1999. Experimental model for studying the primary cilia in tissue culture cells. *Membr. Cell Biol.* 12:895–905.

Anderson, C.T., and T. Stearns. 2009. Centriole age underlies asynchronous primary cilium growth in mammalian cells. *Curr. Biol.* 19:1498–1502. doi:10.1016/j.cub.2009.07.034

Chen, C.S., M. Mrksich, S. Huang, G.M. Whitesides, and D.E. Ingber. 1997. Geometric control of cell life and death. *Science.* 276:1425–1428. doi:10.1126/science.276.5317.1425

Chevrier, V., M. Piel, N. Collomb, Y. Saoudi, R. Frank, M. Paintrand, S. Narumiya, M. Bornens, and D. Job. 2002. The Rho-associated protein kinase p160ROCK is required for centrosome positioning. *J. Cell Biol.* 157:807–817. doi:10.1083/jcb.200203034

Dard, N., S. Louvet-Vallée, A. Santa-Maria, and B. Maro. 2004. Phosphorylation of ezrin on threonine T567 plays a crucial role during compaction in the mouse early embryo. *Dev. Biol.* 271:87–97. doi:10.1016/j.ydbio.2004.03.024

Dawe, H.R., M. Adams, G. Wheway, K. Szymanska, C.V. Logan, A.A. Noegel, K. Gull, and C.A. Johnson. 2009. Nesprin-2 interacts with meckelin and mediates ciliogenesis via remodelling of the actin cytoskeleton. *J. Cell Sci.* 122:2716–2726. doi:10.1242/jcs.043794

Engler, A.J., S. Sen, H.L. Sweeney, and D.E. Discher. 2006. Matrix elasticity directs stem cell lineage specification. *Cell.* 126:677–689. doi:10.1016/j.cell.2006.06.044

Fievet, B.T., A. Gautreau, C. Roy, L. Del Maestro, P. Mangeat, D. Louvard, and M. Arpin. 2004. Phosphoinositide binding and phosphorylation act sequentially in the activation mechanism of ezrin. *J. Cell Biol.* 164:653–659. doi:10.1083/jcb.200307032

Fink, J., M. Théry, A. Azioune, R. Dupont, F. Chatelain, M. Bornens, and M. Piel. 2007. Comparative study and improvement of current cell micropatterning techniques. *Lab Chip.* 7:672–680. doi:10.1039/b618545b

Gerdes, J.M., E.E. Davis, and N. Katsanis. 2009. The vertebrate primary cilium in development, homeostasis, and disease. *Cell.* 137:32–45. doi:10.1016/j.cell.2009.03.023

Graser, S., Y.D. Stierhof, S.B. Lavoie, O.S. Gassner, S. Lamla, M. Le Clech, and E.A. Nigg. 2007. Cep164, a novel centriole appendage protein required for primary cilium formation. *J. Cell Biol.* 179:321–330. doi:10.1083/jcb.200707181

Huang, S., C.S. Chen, and D.E. Ingber. 1998. Control of cyclin D1, p27(Kip1), and cell cycle progression in human capillary endothelial cells by cell shape and cytoskeletal tension. *Mol. Biol. Cell.* 9:3179–3193.

Kim, J., J.E. Lee, S. Heynen-Genel, E. Suyama, K. Ono, K. Lee, T. Ideker, P. Aza-Blanc, and J.G. Gleeson. 2010. Functional genomic screen for modulators of ciliogenesis and cilium length. *Nature.* 464:1048–1051. doi:10.1038/nature08895

McBeath, R., D.M. Pirone, C.M. Nelson, K. Bhadriraju, and C.S. Chen. 2004. Cell shape, cytoskeletal tension, and RhoA regulate stem cell lineage commitment. *Dev. Cell.* 6:483–495. doi:10.1016/S1534-5807(04)00075-9

Mikule, K., B. Delaval, P. Kaldis, A. Jurcyzk, P. Hergert, and S. Doxsey. 2007. Loss of centrosome integrity induces p38-p53-p21-dependent G1-S arrest. *Nat. Cell Biol.* 9:160–170. doi:10.1038/ncb1529

Pan, J., Y. You, T. Huang, and S.L. Brody. 2007. RhoA-mediated apical actin enrichment is required for ciliogenesis and promoted by Foxj1. *J. Cell Sci.* 120:1868–1876. doi:10.1242/jcs.005306

Pardee, A.B. 1974. A restriction point for control of normal animal cell proliferation. *Proc. Natl. Acad. Sci. USA.* 71:1286–1290. doi:10.1073/pnas.71.4.1286

Park, T.J., S.L. Haigo, and J.B. Wallingford. 2006. Ciliogenesis defects in embryos lacking inturned or fuzzy function are associated with failure of planar cell polarity and Hedgehog signaling. *Nat. Genet.* 38:303–311. doi:10.1038/ng1753

Polte, T.R., G.S. Eichler, N. Wang, and D.E. Ingber. 2004. Extracellular matrix controls myosin light chain phosphorylation and cell contractility through modulation of cell shape and cytoskeletal prestress. *Am. J. Physiol. Cell Physiol.* 286:C518–C528. doi:10.1152/ajpcell.00280.2003

Pugacheva, E.N., S.A. Jablonski, T.R. Hartman, E.P. Henske, and E.A. Golemis. 2007. HEF1-dependent Aurora A activation induces disassembly of the primary cilium. *Cell.* 129:1351–1363. doi:10.1016/j.cell.2007.04.035

Santos, N., and J.F. Reiter. 2008. Building it up and taking it down: the regulation of vertebrate ciliogenesis. *Dev. Dyn.* 237:1972–1981. doi:10.1002/dvdy.21540

Schneider, L., C.A. Clement, S.C. Teilmann, G.J. Pazour, E.K. Hoffmann, P. Satir, and S.T. Christensen. 2005. PDGFRalphaalpha signaling is regulated through the primary cilium in fibroblasts. *Curr. Biol.* 15:1861–1866. doi:10.1016/j.cub.2005.09.012

Schwartz, M.A., and R.K. Assoian. 2001. Integrins and cell proliferation: regulation of cyclin-dependent kinases via cytoplasmic signaling pathways. *J. Cell Sci.* 114:2553–2560.

Seeley, E.S., and M.V. Nachury. 2010. The perennial organelle: assembly and disassembly of the primary cilium. *J. Cell Sci.* 123:511–518. doi:10.1242/jcs.061093

Solon, J., I. Levental, K. Sengupta, P.C. Georges, and P.A. Janmey. 2007. Fibroblast adaptation and stiffness matching to soft elastic substrates. *Biophys. J.* 93:4453–4461. doi:10.1529/biophysj.106.101386

Spektor, A., W.Y. Tsang, D. Khoo, and B.D. Dynlacht. 2007. Cep97 and CP110 suppress a cilia assembly program. *Cell.* 130:678–690. doi:10.1016/j.cell.2007.06.027

St Johnston, D., and J. Ahringer. 2010. Cell polarity in eggs and epithelia: parallels and diversity. *Cell.* 141:757–774. doi:10.1016/j.cell.2010.05.011

Tucker, R.W., A.B. Pardee, and K. Fujiwara. 1979. Centriole ciliation is related to quiescence and DNA synthesis in 3T3 cells. *Cell.* 17:527–535. doi:10.1016/0092-8674(79)90261-7

Wheatley, D.N. 1971. Cilia in cell-cultured fibroblasts. 3. Relationship between mitotic activity and cilium frequency in mouse 3T6 fibroblasts. *J. Anat.* 110:367–382.

Wheatley, D.N., E.M. Feilen, Z. Yin, and S.P. Wheatley. 1994. Primary cilia in cultured mammalian cells: detection with an antibody against detyrosinated alpha-tubulin (ID5) and by electron microscopy. *J. Submicrosc. Cytol. Pathol.* 26:91–102.

Zetterberg, A., and O. Larsson. 1985. Kinetic analysis of regulatory events in G1 leading to proliferation or quiescence of Swiss 3T3 cells. *Proc. Natl. Acad. Sci. USA.* 82:5365–5369. doi:10.1073/pnas.82.16.5365